Self-organized nanopatterns in thin layers of superheated liquid metals

E. L. Gurevich*
Leibniz-Institut für Analytische Wissenschaften, ISAS e.V., Dortmund, Germany
(Received 2 September 2010; revised manuscript received 28 October 2010; published 23 March 2011)

In this paper experimental observations of self-organized patterns in resolidified thin films of liquid superheated metals are reported. The superheated melt layers represent an example of a system driven far from equilibrium, which undergoes explosive boiling and solidifies afterward. The melts appear in the course of single-shot femtosecond laser heating of metal samples. Self-organized cells, solitonlike structures, periodic stripes, and transient patterns are observed. Pattern properties and mechanisms leading to the pattern formation as well as possible applications for nanotechnology are discussed.

DOI: 10.1103/PhysRevE.83.031604 PACS number(s): 68.15.+e, 89.75.Kd, 61.25.Mv, 81.16.Dn

I. INTRODUCTION

Recent achievements in nonlinear science have awakened interest in pattern-forming systems of different nature, such as, e.g., chemical, biological, granular, and distributed electric media. Such systems driven far from equilibrium are known to exhibit a large variety of self-organized patterns [1]. Frequently observed are propagating fronts, periodical stripes, hexagonal arrangements, solitons, spirals, and many others. However, some types of patterns are seldom observed in experiments; they are, e.g., the concentric-ring pattern observed only in Rayleigh-Bénard [2] and in gas-discharge [3] systems and self-organized Voronoi diagrams [4] reported in chemical [5] and gas-discharge [6] systems, or by aggregation of crystalline Ge during annealing of an Al/Ge bilayer film deposited on a SiO_2 substrate [7].

A Voronoi diagram (VD) is a partition of an area to a number of domains corresponding to a given set of reference points (nodes). Each domain surrounding a corresponding node consists of points that are closer to the particular node than to any other node. VDs are interesting for practical applications in different branches of science from pattern recognition to partitioning of a city into areas of responsibility for public facilities [8,9]. VDs as a self-organized stationary pattern appear in systems in which the three following conditions are fulfilled: (1) Waves of a certain nature may be excited on a self-organized set of nodes. (2) These waves extend uniformly in all directions. (3) The waves stop as they collide. There are no self-assembled VDs in hydrodynamic systems under normal conditions since there are no *self-assembled* patterns, which could serve as the set of nodes for the waves, and the condition (3) is not fulfilled.

However, these conditions may be fulfilled for superheated liquids. A liquid can be superheated either if there are no nucleation centers, which serve as centers for vapor bubble formation [10], or if the heating is extremely rapid [11], so that the liquid temperature increases more quickly than the characteristic time of the vapor bubble formation. Such liquids in contrast to common ones are almost unexplored due to the complexity of theoretical and experimental techniques. The pattern formation in superheated liquid metals remains completely unexplored up to now, in contrast to classical hydrodynamic systems, where it has been studied since 1834 [12].

In this paper we report on pattern formation in superheated liquid metals. We focus on the formation of self-organized Voronoi-like cells and demonstrate their destabilization to solitonlike structures and periodic stripes. The metal is superheated by exposure to femtosecond laser pulses. As a femtosecond laser pulse impacts the metal surface, the lattice temperature in the surface layer increases at the rate of $\gtrsim 10^{14}$ K/s and exceeds 10^3 K on a subnanosecond time scale [13]. Due to such a quick increase of the surface temperature a thin surface layer undergoes transition to a superheated liquid, which boils explosively [14]. The depth of the liquid layer according to molecular dynamic simulations is approximately several tens of nanometers [13] and 100–200 nm according to simulations based on the two-temperature model [14]; the lateral dimension is close to the laser spot diameter, which is several tens of micrometers. Thus the system at hand is a thin two-dimensional layer of superheated liquid, which undergoes rapid explosive boiling and resolidification.

In our experiments metal samples are exposed to single laser pulses characterized by the following parameters: pulse duration $\tau_p \approx 10^{-13}$ s, pulse fluence on the sample surface F_p varied in the range $F_p = 1$–20 J/cm^2. The femtosecond Ti:sapphire laser system Hurricane with the wavelength of 800 nm produced by Spectraphysics is used. The laser beam is focused on the sample surface in a spot of approximately 40 μm in diameter by means of a UP-XP femtosecond near-ir optical microscope produced by New Wave. Samples of Ag, Al, Au, Cu, Ta, and W of different roughness R (from approximately 30 to 300 nm rms roughness) are studied. The roughness is measured by means ofa Zygo white-light interferometer. The sample surface is always oriented perpendicular to the laser beam. After the interaction with the laser pulse, the sample surface is studied by means of a Quanta 200 F scanning electron microscope (SEM) produced by FEI.

A typical SEM image of the sample surface after the laser processing can be seen in Fig. 1. The surface is covered by a fine network of cells separated by higher edges. The cells appear in different metals under different experimental conditions. There are sharp spikes observed on the intersection points of the edges; see Fig. 1(d). The height of the edges can be estimated by tilting the sample with respect to the electron

*Corresponding author: gurevich@uni-muenster.de

 ©2011 American Physical Society

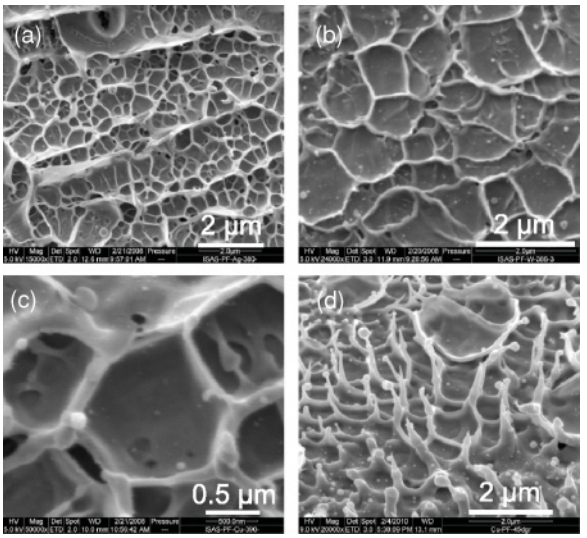

FIG. 1. Voronoi-like cells observed on metallic surfaces after femtosecond laser heating. (a) Ag, $R \approx 120$ nm, $F = 6.3$ J/cm^2; (b) W, $R \approx 200$ nm, $F = 6.3$ J/cm^2; (c) Cu, $R \approx 30$ nm, $F = 6.4$ J/cm^2; (d) Cu, $R \approx 30$ nm, $\alpha = 45°$, $F = 2.5$ J/cm^2.

detector in the SEM at the angle α; see Fig. 1(d) for $\alpha = 45°$. The estimated height of the spikes is up to 3 μm and the thickness is in the range between 100 and 300 nm. The height of the edges is up to 150 nm and the width in the range of 50–100 nm. The tilted image in Fig. 1(d) demonstrates also that the SEM images reflect the real topology of the sample surface but not charging or surface contamination.

The size of the cells may vary from approximately 100 nm to several micrometers depending on the pulse energy and the type of the material. In all experiments radial dependence of the cell size in the laser-affected area on the surface is observed. The cells corresponding to the center of the laser spot are larger than those on the edge of the spot. The radial dependence of the cell size for copper for $F = 6.4$ J/cm^2 and aluminum for $F = 4.7$ J/cm^2 can be found in Fig. 2. Both measured radial dependencies follow the Gaussian profile of

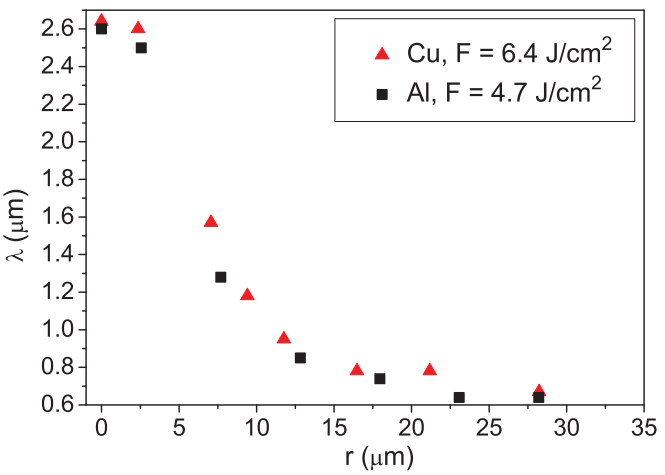

FIG. 2. (Color online) Dependence of the cell size on the radial position in the crater for copper ($R \approx 30$ nm, $F = 6.4$ J/cm^2) and for aluminum ($R \approx 300$ nm, $F = 4.7$ J/cm^2).

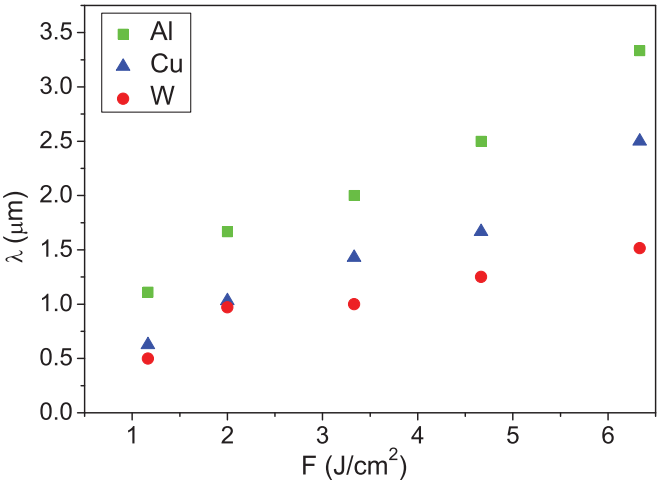

FIG. 3. (Color online) Dependence of the maximal cell size (in the center of the crater) for different metal samples on the pulse fluence.

the laser beam intensity. That is, we can assume that the size of the cells λ monotonically depends on the local laser fluence on the sample surface. Hence, only the cells in the center of the laser spot are considered for comparison of different laser shots. The dependence of the cell size λ on the average pulse fluence F for aluminum, copper, and tungsten samples can be found in Fig. 3. One can see that λ increases nearly linearly with the pulse fluence for all analyzed sample materials.

The size of the cells depends on the properties of the sample material: The cell size for aluminum samples is systematically larger than for copper and tungsten; see Fig. 3. Among the studied materials, silver samples are characterized by the smallest cell size, down to 100–200 nm; see Fig. 1(a). The topology of the pattern does not change with orientation of the sample surface with respect to the gravitational field and is not influenced by the surface roughness.

However, the pattern topology depends on the material properties of the samples. In certain materials the cells are strongly influenced by self-organized periodic stripes or are even completely suppressed by the latter. If a gold surface is processed [see Fig. 4(a), $R \approx 100$ nm], a transient pattern between the stripes and the cells is observed. It is characterized by nearly 120° splitting of the stripes as well as by secondary destabilization of the stripe pattern and appearance of perpendicular ripples of a lower amplitude. In the tantalum sample [see Fig. 4(b)], a periodic stripe pattern partly destabilized by hexagonal cells is found.

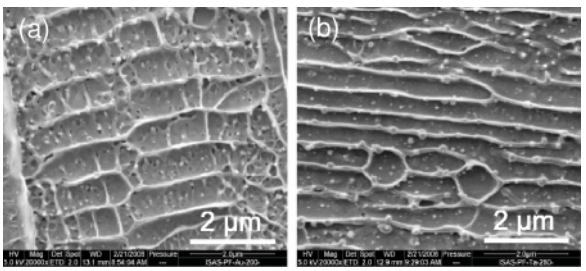

FIG. 4. Formation of periodic stripe pattern. (a) Au, $F = 3.3$ J/cm^2; (b) Ta, $F = 4.7$ J/cm^2.

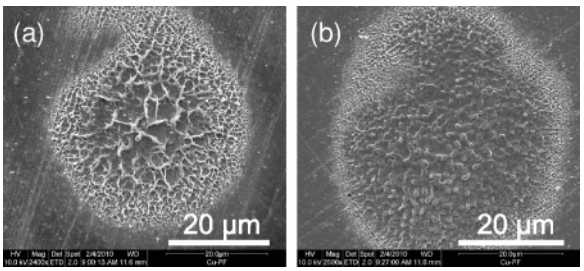

FIG. 5. Copper surface after exposure to one double pulse with (a) $\delta t = 0.5$ s; (b) $\delta t = 6 \times 10^{-9}$ s. The fluence for each single laser pulse within the double pulse $F = 3.0$ J/cm^2 The pulse amplitude variation was less than 10%.

The relation between the cell size and the laser pulse intensity (see Figs. 2 and 3) supports the assumption that the observed cells are formed by the explosive boiling of the superheated melt. Indeed, the size of the cells should grow with the laser fluence (if the density of the seed bubbles is the same), since the bubble growth rate is proportional to the local overheating [15]. This assumption can also be supported by the following two double-pulse experiments: In each experiment the polished copper surface ($R \approx 30$ nm) was exposed to one double pulse consisting of two identical laser pulses with a time interval δt between them. For the first experiment the interval $\delta t = 0.5$ s was achieved by adjusting the open time of a mechanical shutter to the repetition rate of the laser. For the second one $\delta t = 6 \times 10^{-9}$ s was achieved by desynchronization of the Pockels cell delays in the amplifier of the femtosecond laser. The amplitudes and the time delay were monitored by means of a photodiode.

The surface topology for both double-pulse experiments can be found in the SEM image in Fig. 5. One can see that the pattern generated by the double-pulse experiment with the large delay $\delta t = 0.5$ s [see Fig. 5(a)] does not generally differ from the single-pulse pattern (see Fig. 1). After the first laser pulse the sample surface melts and solidifies completely in less than 10 ns; the second laser pulse, which follows after $\delta t = 0.5$ s, also impacts a solid surface. However, as the delay between single laser pulses becomes comparable with the melt time and the second pulse exposes a melt or an incompletely solidified surface, the structure of the resolidified melt becomes different; see Fig. 5(b). The cells are not formed any more and the splash structure consisting of a set of localized patterns is more pronounced. Here the localized spikes are thicker than in the single-pulse heating [see Fig. 1(d)] and cover the whole area of the laser spot.

Although pattern formation in superheated liquid layers has not been explored yet, there are several publications reporting pattern formation by laser ablation of solids: One can observe random splashing patterns [16], concentric rings [17] or periodic stripes, and localized structure there [18]. In the cited papers the self-organized patterns are ascribed to interaction of the incident laser wave with surface defects or with waves of other origin excited on the surface [19,20]. Moreover, in most experiments on pattern formation in laser craters, each surface unit is treated by a large number of laser pulses. This changes the physical mechanisms leading to the pattern formation. Thus, in [18] the authors explain the observed structures by mode-competition models. In the experiments reported in our paper the cells and periodic stripes appear in single-pulse experiments, which simplifies analysis of the underlying physics and excludes mechanisms based on the interaction between subsequent laser pulses. The influence of surface defects [16] is also unlikely since their density is lower than the density of the cells and does not depend on the energy of the laser pulse.

The periodic pattern cannot be attributed to interaction of the laser pulse with surface plasmon waves, since the surface plasmon-polaritons can only be excited either if the surface is periodically patterned or if (i) the surface is irradiated at a certain impact angle $\beta \neq \pi/2$ and (ii) the beam impacts the surface through a medium with refractive index larger than 1. None of these conditions are fulfilled for the system at hand, since the laser beam impacts perpendicular to a smooth surface from the air, whose refractive index is close to unity.

Application of femtosecond lasers for pattern formation experiments simplifies analysis of the background physics considerably for two main reasons: (i) The duration of the laser pulse is shorter than the time needed for formation of the surface acoustic waves. (ii) The pulse duration is also short with respect to the characteristic time scale of the speckle formation; hence the beam profile is speckle-free and the observed pattern is not influenced by low-scale beam inhomogeneities.

The characteristic time and length scales of the hydrodynamic instabilities induced by thermal-noise-induced dewetting of thin liquid layers τ can be estimated by linear stability analysis of the Navier-Stokes equation. The characteristic wave length of the dewetting patterns can be estimated as $\lambda \approx 4h^2\sqrt{\pi^3\gamma/A}$ [21], where $A \sim 10^{-19}$–10^{-20} J is the Hamaker constant, γ the surface tension, and h the depth of the melt layer. For the thickness of the liquid layer $h \sim 10$–100 nm and $\gamma \sim 1$ N/m typical for liquid metals [22], the characteristic size of the pattern should be in the range of 10^{-5}–10^{-3} m. Hence the possible range of the wavelengths of hydrodynamic instabilities for the system at hand is between micrometers and millimeters. Thus, this mechanism may explain the characteristic period of the stripe pattern see (Fig. 4), but not the observed size of the cells (see Fig. 1).

The characteristic time scale for the instability developing due to dewetting of thin liquid films induced by thermal noise can be estimated as $\tau = 3\eta\lambda^4/16\pi^4\gamma h^3 = 48\pi^2\eta\gamma h^5/A^2$. For the melt viscosity $\eta \sim 10^{-3}$ N s/m^2 [22] and $h \sim 10$–100 nm, one can see that τ is of the order of seconds. However, if we suppose that the instability is stopped at an early stage by other mechanisms (such as, e.g., melt resolidification) and the patten stops growing when the pattern size is $\lambda = 0.1$–1 μm as observed in the experiments, the characteristic time can be estimated as $\tau \sim 10^{-10}$–10^{-6} s. The lower limit of this range (corresponding to the cell size $\lambda = 0.1\mu$m) is of the order of 1 ns, which is close to the period of time at which the surface layer remains liquid. The instability time scale τ may be even smaller if one takes into account that the melt viscosity decreases with the temperature. However, large cells in the center of the laser spot cannot be explained in this way, since the hydrodynamic instability has no time to develop and the melt solidifies before the cell grows up to 1 μm.

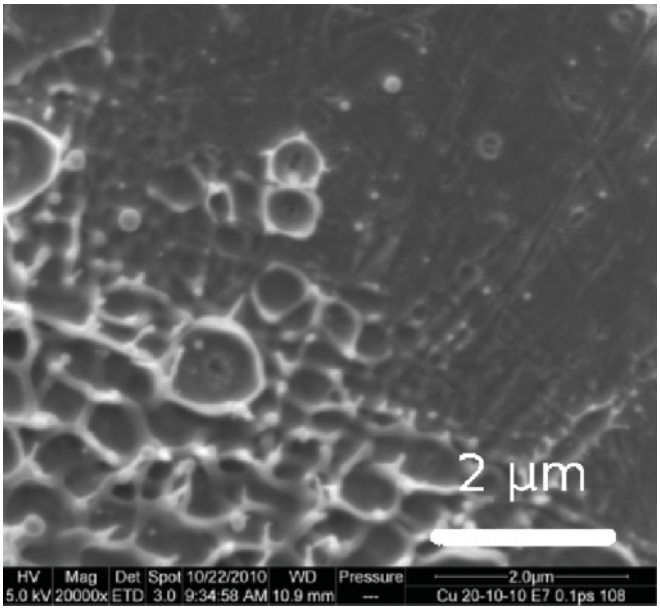

FIG. 6. Cells solidified before extending until the neighboring cells can be found in the peripheral part of the laser crater in copper.

We suppose that the observed pattern is a set of cells with centers in the nucleation centers, which appears in a thin layer of superheated metal melt by explosive boiling. Hence the complete pattern is a self-assembled Voronoi diagram generated by bubbles spontaneously formed in the liquid superheated metals. The bubbles grow until two neighboring bubbles meet and the extension of the Voronoi cell is slowed down and stopped by the pressure in the neighboring cell and by decrease of the vapour pressure with the decreasing temperature [15]. The liquid metal between the nodes is pressed out to the corners of the cells during the cell growth; see Fig. 1(d). Numerical simulations confirm [13,23] that the metal surface is melted during the process of ablation. As the temperature on the surface decreases, the melt pressed between the nodes becomes more viscose and solidifies and a two-dimensional metal foam is formed.

A confirmation of this mechanism can be found in the SEM image (see Fig. 6) made in the peripheral part of the laser crater, where the laser fluence on the sample surface was close to the melting threshold. Here the melt solidifies before neighboring growing bubbles meet. No bubbles smaller than approximately 100 nm have been observed in the experiments. This fits the theory of bubble growth in superheated liquids [15], which suggests that there is a minimal stable size of the seed bubbles. We also note that formation of similar cavities has been observed in molecular dynamics simulations; see, e.g., [13].

The formation of the Voronoi-like cells is influenced by other pattern formation phenomena. We have demonstrated that in certain conditions competition between VDs and periodic stripe pattern takes place. However, the physical background of this secondary destabilization remains unclear since it cannot be attributed to the best-known mechanisms of pattern formation in such systems. Indeed, convection patterns induced by both the Marangoni and Bénard mechanisms develop only if the surface of the liquid film is colder than the bulk, which is not the case for our experiments since the laser radiation heats the sample at the surface. Moreover, the orientation of the sample surface with respect to gravity was found not to influence the pattern, which excludes Bénard convection from the relevant pattern-formation mechanisms. However, influence of the microfluidic instabilities may explain the wavelength of the observed stripe pattern.

The observed structures are interesting for applications, e.g., in nanotechnology for nanopatterning of metallic surfaces or for high-resolution measurements of the laser pulse energy distribution. Artificial introduction of defects on the metal surface suggests the possibility of controlling the positions of the nodes of the Voronoi diagram [24]. It may also be used to investigate characteristics of explosive boiling of superheated liquids such as density of the nucleation centers or the bubble growth rates. In additon, this is an unexplored pattern-forming system, which needs further investigation.

Fruitful discussion with Leonid Zhigilei and Roland Hergenröder is acknowledged.

[1] M. C. Cross and P. C. Hohenberg, Rev. Mod. Phys. **65**, 851 (1993).
[2] K. L. Thompson, K. M. S. Bajaj, and G. Ahlers, Phys. Rev. E **65**, 046218 (2002).
[3] E. L. Gurevich, A. L. Zanin, A. S. Moskalenko, and H.-G. Purwins, Phys. Rev. Lett. **91**, 154501 (2003).
[4] G. Voronoi, J. Reine Angew. Math. **134**, 198 (1908).
[5] B. de Lacy Costello, A. Adamatzky, N. Ratcliff, A. L. Zanin, A. W. Liehr, and H.-G. Purwins, Int. J. Bif. Chaos **14**, 2187 (2004).
[6] A. L. Zanin, A. W. Liehr, A. S. Moskalenko, and H.-G. Purwins, Appl. Phys. Lett. **81**, 3338 (2002).
[7] M. Doi, Y. Suzuki, T. Koyama, and F. Katsuki, Philos. Mag. Lett. **78**, 241 (1998).
[8] A. Okabe, B. Boots, and K. Sugihara, *Spatial Tessellations: Concepts and Applications of Voronoi Diagrams* (John Wiley & Son, Chichester, 1992).
[9] J. Um, S.-W. Son, S. I. Lee, H. Jeong, and B. J. Kim, Proc. Natl. Acad. Sci. USA **106**, 14236 (2009).
[10] D. Zahn, Phys. Rev. Lett. **93**, 227801 (2004).
[11] F. Lang and P. Leiderer, New J. Phys. **8**, 14 (2006).
[12] J. S. Russell, in *Report of the Fourteenth Meeting of the British Association for the Advancement of Science, York, 1844* (AAS, London, 1845), pp. 311–390.
[13] D. S. Ivanov and L. V. Zhigilei, Phys. Rev. B **68**, 064114 (2003).
[14] M. E. Povarnitsyn, K. V. Khishchenko, and P. R. Levashov, Appl. Surf. Sci. **255**, 5120 (2009).
[15] M. S. Plesset and S. A. Zwick, J. Appl. Phys. **25**, 493 (1954).
[16] A. Y. Vorobyev and C. Guo, Opt. Express **14**, 2164 (2006).
[17] F. Ma, J. Yang, X. Zhu, C. Liang, and H. Wang, Appl. Surf. Sci. **11**, 3653 (2010).
[18] O. Varlamova, F. Costache, J. Reif, and M. Bestehorn, Appl. Surf. Sci. **252**, 4702 (2006).

[19] S. A. Akhmanov, V. I. Emel'yanov, N. I. Koroteev, and V. N. Seminogov, Sov. Phys. Usp. **28**, 1084 (1985).
[20] V. N. Tokarev and V. I. Konov, J. Appl. Phys. **76**, 800 (1994).
[21] G. Radson, B. Rumpf, and H. G. Schuster, *Nonlinear Dynamics of Nanosystems* (Wiley-VCH, Weinheim, 2010).
[22] T. Iida and R. I. L. Guthrie, *The Physical Properties of Liquid Metals* (Clarendon Press, Oxford, 1988).
[23] W. H. Duff and L. V. Zhigilei, J. Phys. Conf. Ser **59**, 413 (2007).
[24] E. L. Gurevich, in *Proceedings of the Fourth International Conference on Physics and Control*, edited by L. Fortuna and M. Frasca (Physcon, Catania, Italy, 2009).